

## Turbulence Production by Nonbreaking Waves

I. Savelyev,<sup>1</sup> E. Maxeiner,<sup>2</sup> and D. Chalikov<sup>3,4</sup>

<sup>1</sup>*Remote Sensing Division*

<sup>2</sup>*National Research Council Postdoctoral Associate*

<sup>3</sup>*Swinburne University of Technology, Melbourne, Australia*

<sup>4</sup>*P.P. Shirshov Institute of Oceanology, St. Petersburg, Russia*

**Introduction:** Historically, the parameterization of turbulence production in the upper ocean has relied primarily on the assumptions of near-wall turbulence theory, in which the wind-generated surface friction velocity acts as a moving boundary. In more complete parameterizations, an additional term is added in the top few meters to account for the dissipation of breaking surface waves. These two mechanisms are responsible for the bulk of the produced turbulence. However, there exists a distinct third mechanism, first described by Phillips,<sup>1</sup> in which turbulence is produced due to turbulence interaction with nonbreaking waves. For decades, the contribution of this mechanism was considered relatively small and was therefore largely neglected in practical applications. However, recent studies suggest otherwise. For example, Ardhuin and Jenkins<sup>2</sup> demonstrated that long swell waves propagating across the Pacific Ocean dissipate a significant portion of their energy due to wave–turbulence interaction. These findings motivated the present work, in which a series of laboratory and numerical investigations were conducted to explore this phenomenon. Quantitative results of this study provide a validation source and enable improvements of wave dissipation parameterization, which is needed for accurate marine weather and wave forecasting.

**Laboratory Experiments:** Experiments were conducted in the Free Surface Hydrodynamics Laboratory wave tank (see Fig. 1) at the Naval Research Laboratory in Washington, DC. Starting with quiescent water conditions, nonbreaking waves of small to moderate steepness were generated via sinusoidal motions of the wave paddle. The test area was located ~3.6 m away from the wave maker; test time started upon arrival of first waves and ended before reflected waves from the back wall arrived in the test area.

A priori, near-surface turbulent velocity fluctuations in question were expected to be much smaller than wave orbital velocities, thus falling below detection limits of conventional flow velocimetry techniques. For this reason, a specialized thermal-marking velocimetry (TMV) technique was developed within this study. TMV works by using actively heated points on the water

surface as tracers to visualize and quantify the surface flow. Unlike other floating tracers, thermal markers have the advantage of being minimally invasive to the flow, as well as easily identifiable, renewable, and configurable. Thermal markers were created using a 10-watt CO<sub>2</sub> laser (SYNRAD 48-1) with ~10.6 μm wavelength, which cannot propagate through water and therefore is dissipated into heat at the surface. A motorized mirror, capable of changing its orientation over 1000 times per second, laid down a desired pattern of thermal markers by controlling the direction of the laser beam. A midwave infrared camera (FLIR SC6000) was used to observe water surface temperature and trace movements of thermal markers. An example of an infrared image is shown in Fig. 2, in which vertical dotted lines (initially straight) represent thermal markers, gradually displaced and deformed by the flow. An image-processing algorithm based on a weighted centroid principle was used to analyze pairs of such images and determine marker velocities with a very high accuracy of ±0.8 mm/s, sufficient to detect desired turbulent motion.

**Numerical Model:** The calculations were made with a large eddy simulation (LES) model of 3D non-potential (vortical) motion to represent the turbulence, coupled with a fully nonlinear 2D model of surface waves. Initial conditions were assigned as a train of four harmonic waves using small amplitude theory. Initial turbulence was introduced as a field of random velocities satisfying the continuity equation. Total initial turbulent energy was set equal to 0.001 of the total wave energy. Since the energy of vortical motion is much smaller than the energy of the waves, the back transfer of energy to waves and attenuation of waves due to dissipation were neglected. Using the periodic boundary condition, waves were allowed to propagate for the duration of up to 10 wave periods.

**Results:** In both numerical and laboratory simulations, the turbulent kinetic energy (TKE) was found to grow in time, due to the wave–turbulence interaction. The growth of horizontal components of TKE, i.e.,  $u_x^2$  and  $u_y^2$ , observed in the wave tank is shown in Fig. 3. Interestingly, the cross-tank  $y$  velocity component was found to be more energetic than the  $x$  component. A numerical result of TKE dependence on wave phase is shown in Fig. 4. This result demonstrates that the turbulence is most energetic near wave crests, but quickly decays toward troughs. It also confirms  $y$  component dominance over  $x$ . The reason for this anisotropic behavior can be related to dark and bright bands seen in Fig. 2. These bands correspond to cool skin temperature fluctuations known to be disrupted by near-surface vortex pairs elongated in the streamwise direction.

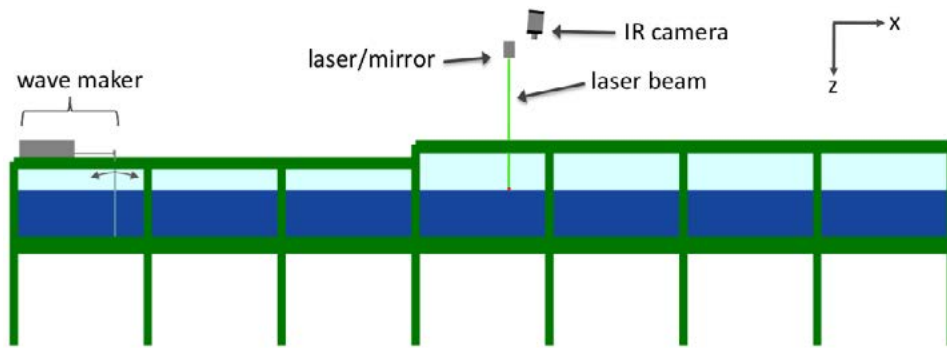


**FIGURE 1**  
Schematic illustration of wave tank and experimental setup. Tank dimensions are 8.5 m long by 2.3 m wide with 0.75 to 0.9 m high transparent sidewalls. The test area is located 3.6 m from the wave maker and 4.0 m from the back wall.

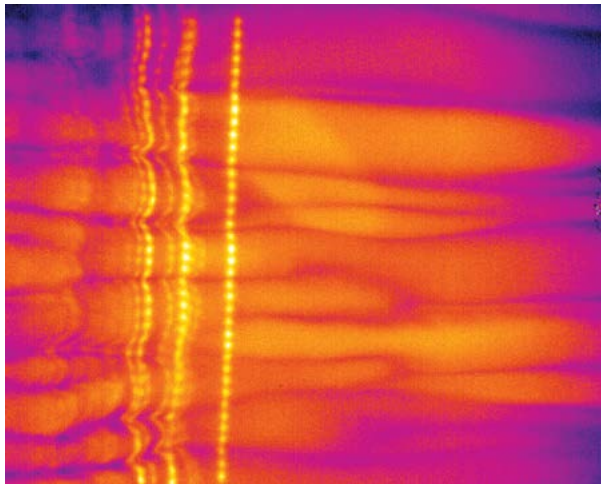


**FIGURE 2**  
An example of a raw 25 × 31 cm infrared image of the water surface with observed thermal streaks. Waves are propagating from right to left. Image brightness represents water temperature, ranging within ~1 °C. Vertical bright dotted lines are thermal markers, and horizontal streaks correspond to elongated near-surface eddies. The oldest thermal markers are located on the left and the most recent ones are on the right.

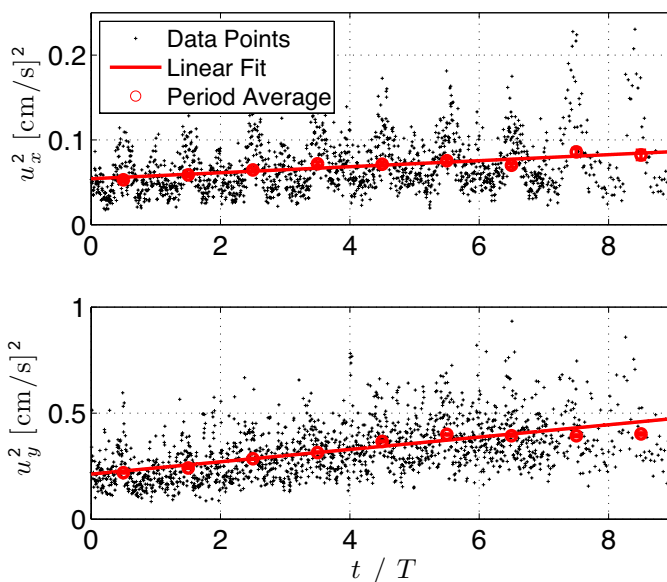


**FIGURE 3**  
Turbulent components of the surface velocities  $u_x^2$  and  $u_y^2$  are shown as functions of time normalized by wave period  $t/T$  for the entire data set. Each point is a bin average over 50 realizations, the solid line is a linear fit through all realizations, and circles are averages over each wave period.

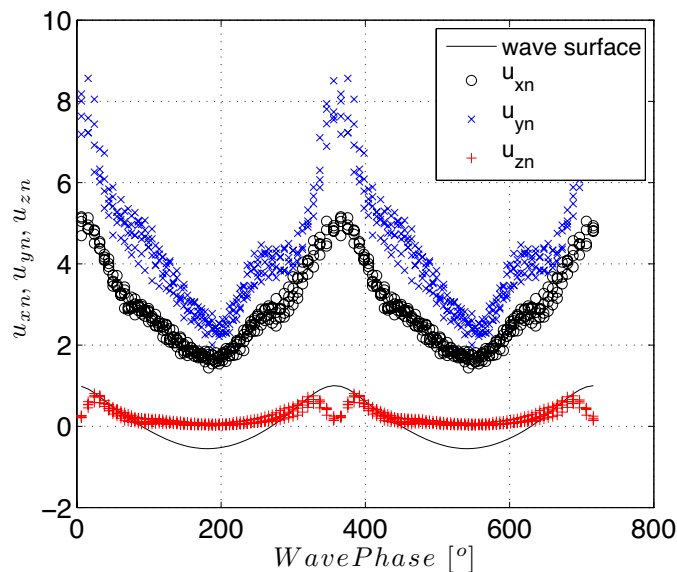


**FIGURE 4**  
Numerical simulation of normalized turbulent velocities, shown as functions of wave phase. Solid line corresponds to the normalized wave-shape, with wave steepness at  $ak = 0.167$ .

Such circulation patterns are expected to favor velocities in  $y$  direction over  $x$ . More details on this study can be found in Savelyev et al.<sup>3</sup>

**Acknowledgments:** Numerical simulations were contributed by Dmitry Chalikov.  
[Sponsored by the NRL Base Program (CNR funded)]

#### References

- <sup>1</sup> O. Phillips, "A Note on the Turbulence Generated by Gravity Waves," *J. Geophys. Res.* **66**(9), 2889–2893 (1961).
- <sup>2</sup> F. Ardhuin and A. Jenkins, "On the Interaction of Surface Waves and Upper Ocean Turbulence," *J. Phys. Oceanogr.* **36**, 551–557 (2006).
- <sup>3</sup> I.B. Savelyev, E. Maxeiner, and D. Chalikov, "Turbulence Production by Nonbreaking Waves: Laboratory and Numerical Simulations," *J. Geophys. Res.* **117**, C00J13 (2012).




---



---

## A Target Depth Classification Method for Autonomous Passive Acoustic Surveillance Systems in Littorals

A. Turgut and L.T. Fialkowski  
*Acoustics Division*

**Introduction:** A robust depth-discrimination method is being developed for passive target classification that provides an autonomous, pervasive, and persistent surveillance capability to the Navy. The new method, appropriate for littoral environments, is based on waveguide invariant theory that requires minimal environmental information and determines if a distant sound source is near the surface or submerged. A two-class discrimination problem is solved using measured acoustic intensity interference patterns; the method

is suitable for existing passive surveillance systems such as horizontal hydrophone arrays or distributed networks of acoustic sensors. The method was successfully validated in a Littoral Depth Discrimination Experiment (LIDDEX12), where shallow and deep sound sources were towed simultaneously and Expendable Mobile ASW Training Targets (EMATTs) were used. Potential applications of the new method are the identification of submarine surges from ports and force protection in ports and harbors.

**Autonomous Passive Acoustic Surveillance:** Current approaches for depth discrimination in littorals are based on extensions of matched-field processing to more robust methods, such as acoustic mode scintillation<sup>1</sup> and acoustic mode filtering.<sup>2</sup> These methods rely on environmental inputs and vertical receiver arrays, neither of which are practical nor considered for surveillance systems. Littoral environments are spatially, temporally, and seasonally dynamic; surveillance applications require robustness to these variations in order to achieve a sufficient level of autonomy. The NRL Acoustics Division is developing and validating different waveguide-invariant-based methods that are suitable for littoral environments. These methods show great potential for passively depth-discriminating quiet submerged targets over wide littoral areas. Field experiments will be used to validate the methods for extreme littoral environmental conditions: summer and winter. This article describes experimental validation of one method and discusses its potential use for autonomous passive acoustic surveillance systems.<sup>3,4</sup>

**LIDDEX12 Summer Experiment:** The objective of the LIDDEX12 experiment was to validate waveguide-invariant-based depth-discrimination algorithms for

passive sonar in shallow water in a summer environment. The experiment took place August 24 through 31, 2012, on the New Jersey Shelf, where available broadband noise from surface ships of opportunity and controlled acoustic sources were recorded on several experimentally deployed receiver arrays (Fig. 5): a bottom-moored 64-element L-shape (horizontal and vertical) receiver array, four Environmental Acoustic Receiver Systems (EARS), and several sonobuoys. To validate target depth classification algorithms, coherent acoustic data (300 to 1200 Hz) from shallow- and deep-towed sources, as well as acoustic data from quiet EMATTs, were used. Additionally, oceanographic data were collected using Conductivity, Temperature, and Depth (CTD) casts, thermistor arrays, and towed CTDs. The high-quality acoustic measurements, along with the time-coincident oceanographic measurements, will be used to demonstrate the robustness of waveguide-invariant-based passive target classification in complex shallow-water environments.

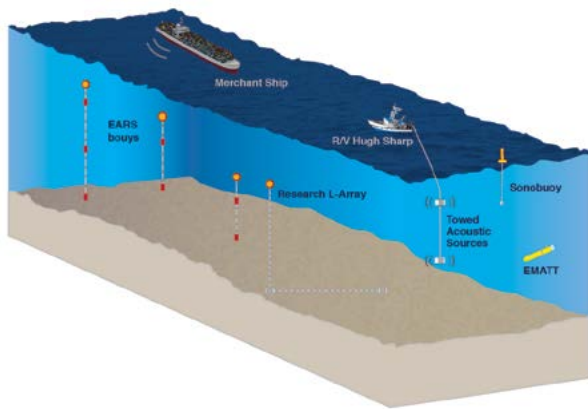


**FIGURE 5**  
LIDDEX12 used a bottom-moored combined horizontal and vertical array, bottom-moored vertical arrays, as well as sonobuoys to record acoustic transmissions from two low-level controlled sources at variable depths, EMATTs, and surface ships-of-opportunity.

The ocean thermocline is a transition layer between the warmer surface water (mixed layer) and the cooler deeper water, and is present in littorals from early spring to late fall. The presence of the ocean thermocline provides an opportunity for passive depth classification through the waveguide parameter,  $\beta$ . Figures 6(a) and 6(b) show measured broadband striations from the controlled sources that were towed at a deep depth (below the thermocline) and at a shallow depth (above the thermocline). The slope of the striations is different for each of these sources, and is related to the depth diversity of the waveguide invariant. For comparison, Fig. 6(c) shows measured broadband striations from the tow ship, the R/V *Sharp*. Note

that the slope of the striations from the R/V *Sharp* is similar to the slope of the striations from the shallow source. The broadband striation patterns of each source are analyzed to provide an estimate of the waveguide invariant parameter,  $\beta$ , through the application of a Hough transform. The result is a waveguide parameter distribution function, shown in Fig. 6(d). The estimate of the waveguide invariant distribution for the shallow source is the red curve, while the estimate for the deep source is the black curve. One example classification implementation of these waveguide distribution estimates is the use of a receiver operating characteristic (ROC) curve, as seen in Fig. 6(e). In this case, the ROC curve is a parametric plot of correct classification probability ( $P_{cc}$ ) versus false classification probability ( $P_{fc}$ ), and is generated from the probability density estimates in Fig. 6(d). The classifier ROC curve is obtained as a cumulative distribution by varying the threshold over the expected range of possible  $\beta$  values. An ROC curve that follows the left then top border of the ROC space is indicative of an accurate metric, while an ROC curve that is close to a 45° diagonal is considered an inaccurate metric. The ROC curve in Fig. 6(e) shows that the waveguide invariant distribution is an appropriate method for accurate depth classification in the littoral environment tested. Further validation studies are being performed using broadband noise data measured during LIDDEX12, and verified to originate from merchant ships identified by Automatic Identification System (AIS) contacts. Figure 7(a) shows broadband striations originating from a merchant ship, measured on a bottom-moored hydrophone. Figure 7(b) shows the corresponding waveguide parameter distribution function, calculated by the application of a Hough transform and incorporation of the ship navigation data from AIS. The resulting waveguide parameter distribution for this distant ship is consistent with that of the shallow source in Fig. 6(d) (red line).

**Summary:** Waveguide-invariant-based methods are being developed at NRL that use a minimal amount of environmental information that is readily available from archival data: the water depth and the depth of the ocean thermocline. One waveguide invariant depth classification method has been validated with a single sensor placed below the ocean thermocline. Analysis of horizontal array data is under way to validate this method for depth classification of ultraquiet targets that cannot be achieved with a single phone. The newly developed methods will be further validated using acoustic data from existing surveillance systems.

[Sponsored by the NRL Base Program (CNR funded)]

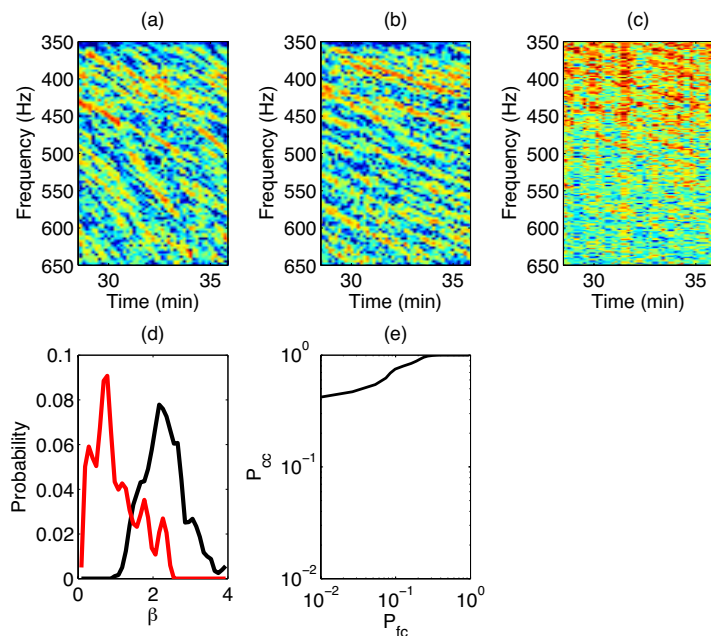


**FIGURE 6**  
 Top row: measured broadband striations from (a) deep source, towed below the thermocline, (b) shallow source, towed above the thermocline, and (c) R/V *Sharp*, the tow ship (also above the thermocline). Bottom row: (d) waveguide parameter distributions for a shallow source (red) and deep source (black), and (e) the ROC curve based on the two distributions.

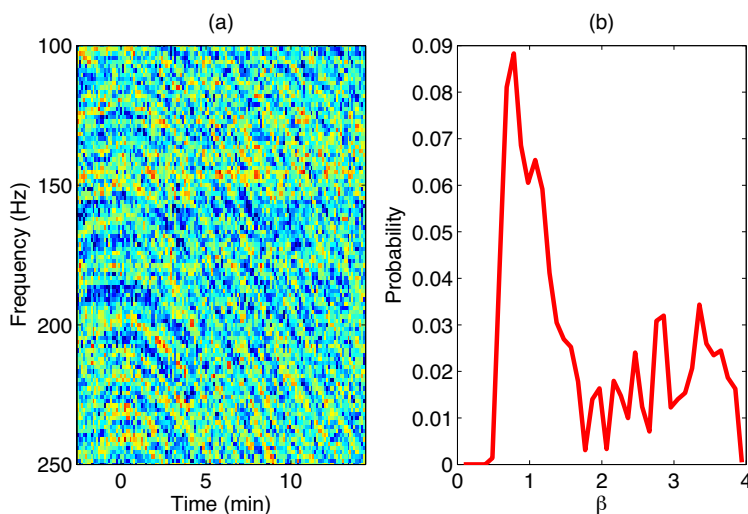


**FIGURE 7**  
 (a) Measured broadband striations from a merchant ship and (b) corresponding waveguide parameter distribution function.

## References

- <sup>1</sup> V.E. Premus, "Modal Scintillation Index: A Physics Based Statistic for Acoustic Source Discrimination," *J. Acoust. Soc. Am.* **105**(4), 2170–2180 (1999).  
<sup>2</sup> V.E. Premus, J. Ward, and C.D. Richmond, "Mode Filtering Approaches to Acoustic Source Depth Discrimination," Conference Record of the Thirty-Eighth Asilomar Conference on Signals, Systems and Computers, Nov. 7–10, 2004, Vol. 2, pp. 1415–1420 (IEEE, 2004).

- <sup>3</sup> A. Turgut and L.T. Fialkowski, "Depth Discrimination Using Waveguide Invariance," *J. Acoust. Soc. Am.* **132**(3), Pt. 2, 2054 (2012).  
<sup>4</sup> A. Turgut and L.T. Fialkowski, "Method and Apparatus for Depth Classification in Shallow Water," Naval Research Laboratory Patent Disclosure, 2012.



## Maximizing Effectiveness of Autonomous Underwater Vehicles

L.F. Smedstad,<sup>1</sup> C.N. Barron,<sup>1</sup> K.D. Heaney,<sup>2</sup>

G. Peggion,<sup>3</sup> and E.M. Coelho<sup>3</sup>

<sup>1</sup>*Oceanography Division*

<sup>2</sup>*Ocean Acoustical Services and Instrumentation Systems, Inc. (OASIS)*

<sup>3</sup>*University of New Orleans*

**Introduction:** Ocean gliders and other unmanned underwater vehicles play an increasingly important role for the U.S. Navy as a source of targeted environmental measurements. Glider pilots adjust navigation instructions for each platform in response to changing array distribution and local ocean conditions. Automated guidance for glider missions enables more effective use of growing numbers of ocean gliders without overtaxing limited human resources. NRL-developed systems to optimize glider placement and sampling direction initiated under the Office of Naval Research (ONR) Glider Observation Strategies (GOST) project have been transitioned to the Naval Oceanographic Office (NAVOCEANO). GOST is an autonomous system that develops preferred deployment and navigation plans for glider networks. GOST uses a genetic algorithm (GA)<sup>1</sup> that sorts through potential waypoints to identify glider paths that achieve optimal coverage. Under this approach, the relative merits of alternate pathsets are calculated using mission-appropriate cost functions that combine geographic coverage, forecast uncertainty, and environmental variability. Feedback from GOST-directed gliders into ocean models demonstrated improved ocean forecast skill in two NATO exercises, REP10 and Proud Manta 11. NAVOCEANO will conduct operational tests of the GOST system during the Navy's Trident Warrior 13 exercise.

**Application of a Genetic Algorithm to Oceanography:** GOST begins with the fundamental postulate that some sets of glider trajectories will be more useful than others. Once the relative merit of a potential set of observations can be quantified, a search algorithm can be implemented to isolate a preferred set. GOST communicates these preferences using cost functions that assign a value based on the time, location, and collective coverage of the glider array. Integrating the vector sum of the velocity and ocean currents reveals the series of observations that could be obtained by a glider. Included in GOST is the Environmental Measurements Path Planner (EMPath) software that contains the GA. Promoting a "survival of the fittest" approach, a randomized set of individuals and a specified number of reproductions (mating of successful individuals) creates generations of a solution. Each individual represents

a different time/space transect pattern for multiple gliders, or sensor laydown, and the natural selection process deems which is best adapted for the mission criteria. EMPath outputs include a morphology figure to provide the user a visual level of confidence in the paths. The morphology computation is an estimate of the shape of the cost function that the genetic algorithm is using to optimize sensor locations. The preferred set of trajectories is communicable to the glider pilots as a set of waypoints and tolerances.

**Benefit to Ocean Models and Tactical Decision Aids:** The effectiveness of GOST guidance has been demonstrated in virtual and live glider exercises in which glider measurements are assimilated as vertical profile data to influence ocean forecasts. Coverage missions include time scales from days to weeks. A set of idealized Observation System Simulation Experiments (OSSEs) form the basis for the GOST 1.0 validation testing.<sup>2</sup> Acoustic products such as sonic layer depth (SLD) created from Relocatable Circulation Prediction System Navy Coastal Ocean Model (RELO NCOM) outputs are analyzed with and without glider assimilation. An assimilative RELO NCOM run designated as the true ocean state has relatively shallow SLD (Fig. 8(a)), while a nonassimilative version with overly deep SLD is the forecast that badly needs correcting (Fig. 8(b)). Using cost functions based on RELO NCOM forecast fields, GOST determines preferred trajectories for six simulated gliders that sample the true ocean. Assimilation of the glider profiles produces the beginnings of a clear correction (Fig. 8(c)) in the target area SLD forecast.

GOST-determined sampling in two NATO exercises has demonstrated the impact of glider observations on target-area forecasts. In the Marine Rapid Environmental Assessment (REP10) exercise off La Spezia, Italy, in August, 2010, the effectiveness of a single GOST-directed glider, known as Laura, relative to an alternative fixed survey with other sensors<sup>3</sup> reduced the maximum and mean root mean square (rms) errors relative to independent observation and more accurately located a cyclonic eddy on the western edge of the target area (Fig. 9). A similar exercise off the east coast of Sicily (Proud Manta 11) showed the effectiveness of GOST guidance for a pair of gliders. The glider sampling identified a previously undetected cold-core ring that significantly modified sound speed and acoustic transmission across the target area (Fig. 10).

**Future Work:** Additional work has begun on expanding the usefulness of a system of gliders with the Navy goals of tactical operations, sustained coverage, and feature definition in mind. All three of these have been present in some capacity on the NATO exercises. However, more automation and management of glider

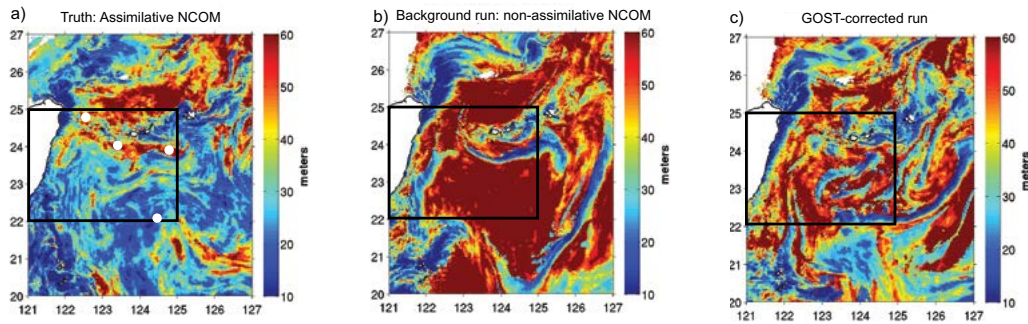


**FIGURE 8**

Sonic layer depth (SLD) has large differences between the case (a) assimilative run taken to represent the true ocean and the case (b) nonassimilative background run. GOST simulates glider observations (a; white circles) of the true ocean. When these are assimilated, the GOST-corrected forecast case (c) moves from deep background SLD (red) to the shallower SLDs (blue) found in the truth ocean, enabling more accurate predictions of upper-ocean acoustic transmission in the target area box.

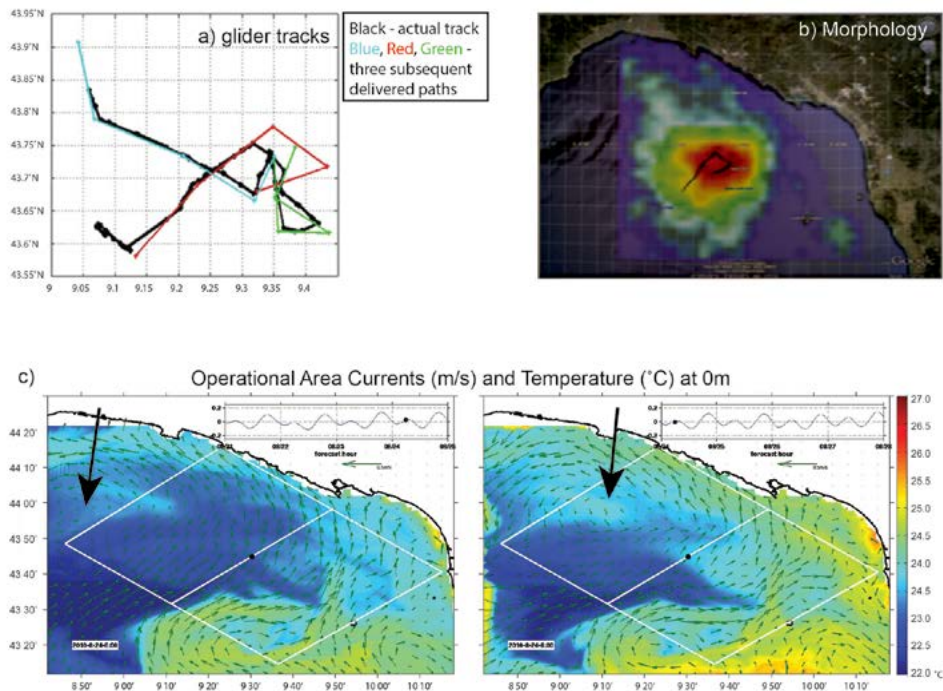


**FIGURE 9**

The feedback between gliders and models is shown from REP10 results. (a) Forecast target waypoints for glider Laura were delivered every 48 hours. The actual trajectory of Laura over the week is shown in black. The gliders were able to follow suggested paths (b) based on the cost function morphology as projected in Google™ Earth. (c) Assimilating glider data improved the forecast location of an eddy (arrows) in the model between a 78-hour forecast and a 6-hour forecast.

data is required. Additional testing of newer capabilities with EMPATH can be conducted, such as roping off areas to protect gliders from entering naturally or politically hostile areas by geographic exclusion zones or other water space limitations. New options are in development to extend forecast horizons and facilitate glider rendezvous to reduce recovery time and cost at mission end. Optimized use of the expanding glider fleet is only possible with such systems to simplify control and management of these resources.

**Acknowledgments:** The authors wish to thank Peter Spence and David Sitton of Qinetiq North America for support in development of model inputs for EMPATH testing, Jan Dastugue of NRL for graphics support, Robert Helber of NRL for acoustical analysis routines, Clark Rowley of NRL for RELO NCOM development, and Richard Campbell of OASIS for EMPATH support.

[Sponsored by ONR]

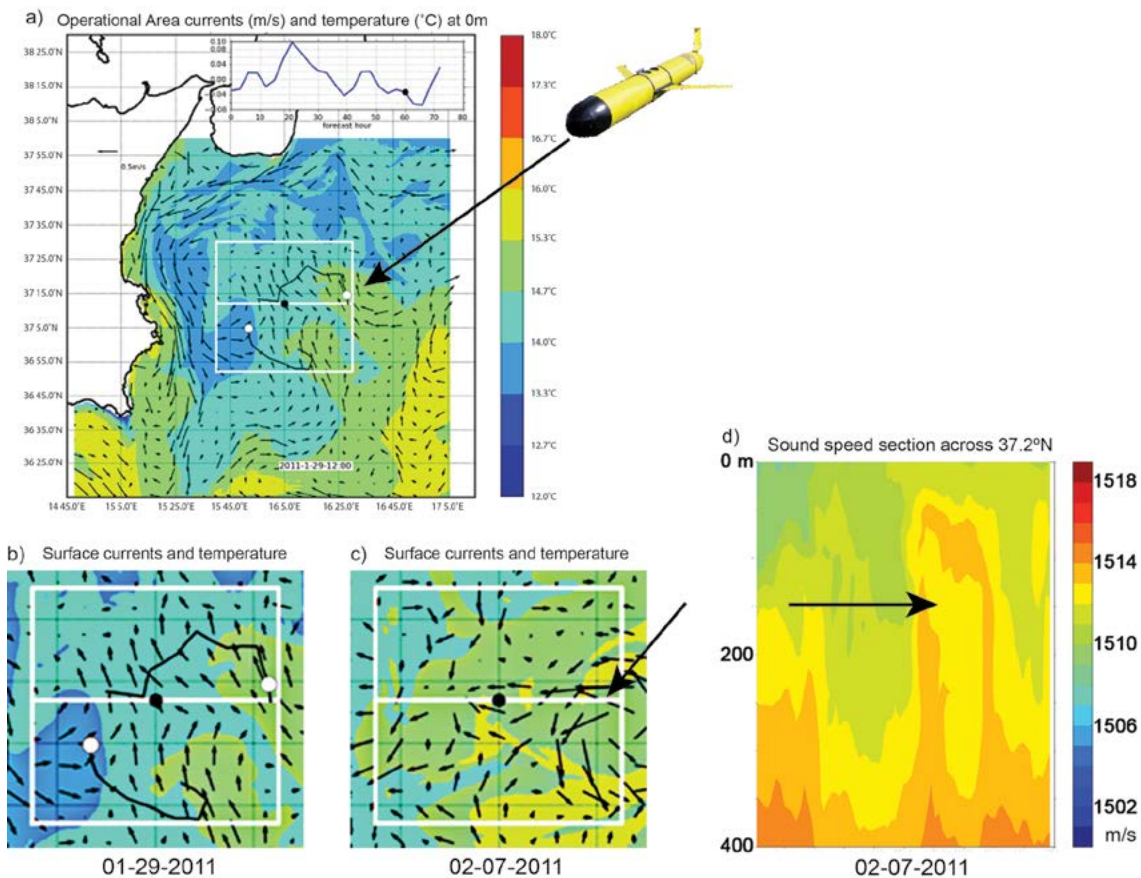


**FIGURE 10**  
 Example of feature definition mission: Surface currents and temperature before (a,b) and after (c,d) assimilation of observations from GOST-directed gliders during the NATO exercise Proud Manta in 2011 off the east cost of Sicily. The gliders identified a cold-core ring (arrows) that significantly modifies currents (c) and sound speed (d) in the operational area.

## References

- <sup>1</sup> K.D. Heaney, G. Gawarkiewicz, T.F. Duda, and P.F.J. Lermusiaux, "Nonlinear Optimization of Autonomous Undersea Vehicle Sampling Strategies for Oceanographic Data-Assimilation," *Journal of Field Robotics* **24**, 437–448 (2007).
- <sup>2</sup> L.F. Smedstad, K.D. Heaney, G. Peggion, C.N. Barron, and E. Coelho, "Validation Test Report for a Genetic Algorithm in the Glider Observation Strategies (GOST 1.0) Project: Sensitivity Studies," NRL/MR/7320--12-9361, Naval Research Laboratory, Stennis Space Center, MS, 2012.
- <sup>3</sup> A. Alvarez and B. Mourre, "Oceanographic Field Estimates from Remote Sensing and Glider Fleets," *J. Atmos. Oceanic Technol.* **29**, 1657–1662 (2012).



## WAVEWATCH III® Transition to Naval Operations

J.D. Dykes and W.E. Rogers  
*Oceanography Division*

**Supporting the Mission:** Knowledge of the sea state and thus predictions of wave conditions in real

time are important for naval operations. Two operational centers provide such support. Fleet Numerical Meteorology and Oceanography Center (FNMOC) in Monterey, California, produces and delivers wave forecasts covering large spatial scales and long time scales — for example, global 120-hour forecast fields of significant wave height — to support general operations. The Naval Oceanographic Office (NAVOCEANO) at Stennis Space Center, Mississippi, provides small-scale wave forecasts covering shorter intervals to support specific missions involving littoral waters and surf zones.

The Naval Research Laboratory (NRL) at Stennis Space Center has been the primary transition partner with NAVOCEANO and FNMOC for enabling technologies in wave forecasting for small and large scales. Now, in cooperation with the National Centers for Environmental Prediction (NOAA/NCEP), the latest version (v. 4.10) of the WAVEWATCH III® (WW3) wave model is being transitioned to NAVOCEANO and FNMOC, with additional updates coming later in 2013.

As part of this transition, NRL has developed and tested a system that uses the multi-grid implementation of WAVEWATCH III® at NAVOCEANO as an improvement to the current systems in place; NAVOCEANO runs a set of large-scale domains around the world to provide wave energy boundary conditions to smaller scale regional wave models. In addition, NRL is providing upgrades to the system to include curvilinear gridded domains, e.g., to cover the Arctic Ocean.

**Multi-grid Model:** WAVEWATCH III®<sup>1,2</sup> is a third-generation wave model developed at NOAA/NCEP that incorporates sophisticated features not available in predecessors, such as modular Fortran90 and highly scalable parallel programming, dynamic time-stepping, third-order propagation schemes, irregular grids, triangular grids, and two-way communication between domains. The model solves the random phase spectral action density balance equation for wavenumber-direction spectra. Being a phase-averaged model, there is an implied assumption that properties of the forcing, as well as the wave field itself, differ on space and time scales that are much larger than individual waves.

During the past five years, WW3 has evolved such that it can now be regarded as a community model, though primary responsibility and authority for the code is still with NOAA/NCEP, and is freely available as Version 3. The development code currently designated as Version 4 is being used to update systems operational in the U.S. Navy. For wind input, wave breaking, and swell dissipation source functions, the physics package of Ardhuin et al.<sup>3</sup> will be used.

The multi-grid (or mosaic grid) feature of WW3 allows for the two-way communication of energy across domain boundaries. Traditionally, as it is with older versions of WW3, a low-resolution host model passes wave energy through the boundary to high-resolution nest domains and whatever happens within the nest domains does not affect the host. With two-way communication, the predictions from the high-resolution model — potentially using better winds and better bathymetry — are shared with what could be considered the host domain and other high-resolution domains. Figure 11 illustrates this.

The current real-time configuration includes a global domain with 0.5° resolution and nine regional domains with resolutions of either 0.1° or 0.2°. Figure 12 illustrates the layout of all the domains. Winds forcing the global domain come from the Navy Global Environmental Model (NAVGEM) and the winds for the regional domains come from the Coupled Ocean/Atmosphere Mesoscale Prediction System (COAMPS™), both running at FNMOC. This modeling system now runs on an IBM iDataPlex Linux system at the Navy DoD Supercomputing Resource Center, where fore-

cast grids of significant wave height, wave direction, and wave period are produced automatically every 12 hours.

In addition, in a recent version developed at NRL, it is now possible that domains with dissimilar grid types (e.g., curvilinear grids and regular grids) can be run together, passing wave energy across the boundaries in both directions, as illustrated in Fig. 13. This removes the problem of running a regular latitude-longitude mesh too far north, decreasing the need to run a very small time step to accommodate for the convergence of the meridians. An Arctic curvilinear mesh can be incorporated into the operational system just like any of the other domains.

**Implications and Conclusion:** One advantage to running the multi-grid version of WW3 is that domain configuration is more efficient than in conventional methods, using computational resources more where needed, i.e., minimizing the redundancy. Any given geographic location is modeled by only one grid point except where there is overlap within buffer zones around boundaries. Compared to a conventional setup, the current configuration turnaround time has improved by about a factor of 3.

Since the multi-grid system runs multiple domains together instead of the traditional approach of running individual domains separately and sequentially, the model setup is less tedious, obviating the need to specify individual points in the host domain about the nest to which information is to be shared.

Comparisons of WW3 wave height output were made with in situ observations and altimeter measurements. Statistics from a number of buoy wave measurements provided by the NOAA Data Buoy Center (NDBC) and plotted in terms of mean bias, standard deviation, correlation coefficient, slope, and scatter index showed good results.

With the transition of the WW3 multi-grid system, wave modeling will be more streamlined, saving processing time, and forecast accuracy is expected to improve.

**Acknowledgments:** The authors thank Paul Wittmann for his advice during the WW3 transition. Funding provided by the Office of Naval Research through the National Oceanographic Partnership Program for continued development of WW3 is appreciated.

[Sponsored by ONR]

#### References

- <sup>1</sup>H.L. Tolman, B. Balasubramanian, L.D. Burroughs, D.V. Chalikov, Y.Y. Chao, H.S. Chen, and V.M. Gerald, "Development and Implementation of Wind-Generated Ocean Surface Wave Models at NCEP" *Weather and Forecasting (NCEP Notes)* 17, 311–333 (2002).

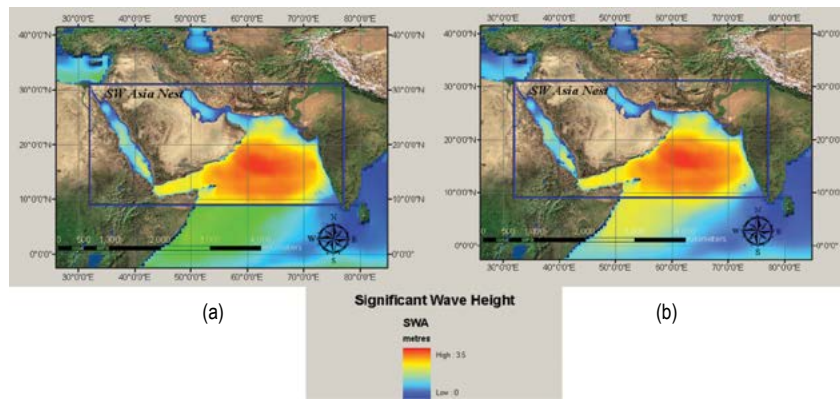


**FIGURE 11**  
 Example of a domain where in (a) one-way nesting occurs, while in (b) two-way nesting is implemented in the multi-grid model.

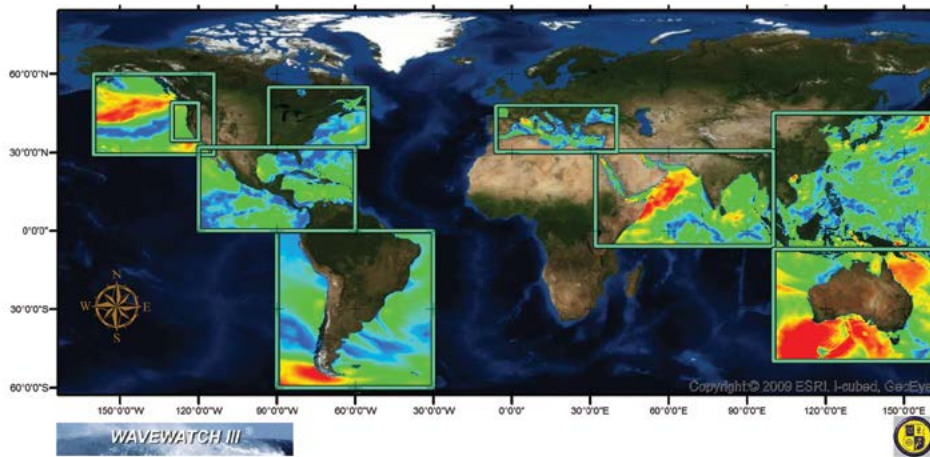


**FIGURE 12**  
 Global and regional domains used primarily for providing boundary conditions for smaller scale models.

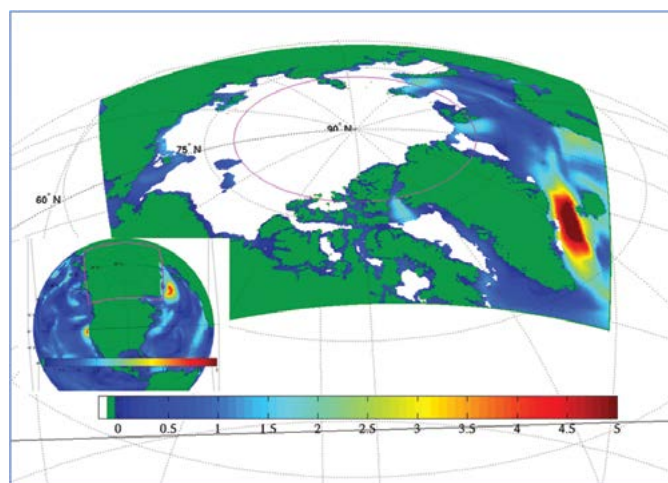


**FIGURE 13**  
 Two-way nesting test with the curvilinear grid Arctic domain (~16 km resolution) and full (0.5°) global domain. Wave height is in meters. The regular global domain is plotted in the inset where masked areas shown in green include the land, ice, and the Arctic domain.

<sup>2</sup> H.L. Tolman, "User Manual and System Documentation of WAVEWATCH III® Version 3.14," Tech. Note, NOAA/NWS/NCEP/MMAB, 220 pp. (2009).

<sup>3</sup> F. Ardhuin, W.E. Rogers, A. Babanin, J.-F. Filipot, R. Magne, A. Roland, A. van der Westhuysen, P. Queffelec, J.-M. Lefevre, L. Aouf, and F. Collard, "Semi-empirical Dissipation Source Functions for Ocean Waves: Part I, Definitions, Calibration and Validations," *J. Phys. Oceanogr.* **40**, 1917–1941 (2010). ◆